

Nanoscale

Accepted Manuscript



This is an *Accepted Manuscript*, which has been through the Royal Society of Chemistry peer review process and has been accepted for publication.

Accepted Manuscripts are published online shortly after acceptance, before technical editing, formatting and proof reading. Using this free service, authors can make their results available to the community, in citable form, before we publish the edited article. We will replace this *Accepted Manuscript* with the edited and formatted *Advance Article* as soon as it is available.

You can find more information about *Accepted Manuscripts* in the [Information for Authors](#).

Please note that technical editing may introduce minor changes to the text and/or graphics, which may alter content. The journal's standard [Terms & Conditions](#) and the [Ethical guidelines](#) still apply. In no event shall the Royal Society of Chemistry be held responsible for any errors or omissions in this *Accepted Manuscript* or any consequences arising from the use of any information it contains.

ARTICLE

Instant Gelation Synthesis of 3D Porous MoS₂@C Nanocomposites for Lithium Ion Batteries

Cite this: DOI: 10.1039/x0xx00000x

Ling Fei^a, Yun Xu^a, Xiaofei Wu^a, Gen Chen^a, Yuling Li^a, Binsong Li^b, Shuguang Deng^a, Sergei Smirnov^c, Hongyou Fan^b, and Hongmei Luo^{a*}

Received 00th October 2013,

Accepted 00th

DOI: 10.1039/x0xx00000x

www.rsc.org/

Abstract: Three-dimensional (3D) nanoporous architectures, possessing high surface area, massive pores, and excellent structural stability, are highly desirable for many applications including catalysts and electrode materials in lithium ion batteries. However, the preparation of such materials remains a major challenge. Here, we introduce a novel method, instant gelation, for the synthesis of such materials. The as-prepared porous 3D MoS₂@C nanocomposites, with layered MoS₂ clusters or strips ingrained in porous and conductive 3D carbon matrix, indeed showed excellent electrochemical performance when applied as anode materials for lithium ion batteries. Its interconnected carbon network ensures good conductivity and fast electron transport; the micro-, and mesoporous nature effectively shortens the lithium ion diffusion path and provides room necessary for volume expansion. The large specific surface area is beneficial for a better contact between electrode materials and electrolyte.

1. Introduction

There are surging demands to develop rechargeable lithium ion batteries (LIBs) with high energy and power density for various applications including clean-energy technologies (e.g. electric vehicles (EVs)) and intermittent renewable energy generation systems (e.g. solar and wind energy).¹⁻³ Unfortunately, the low theoretical capacity (372 mAh g⁻¹) of commercial graphite anode limits the further development of LIBs. Exploring new electrode materials with low cost and light weight while delivering high capacity as well as long cycle life, lies in the central for advancing LIBs technology.⁴⁻⁷ Recently, molybdenum disulfide (MoS₂), showing outstanding catalytic, tribological, and electrochemical properties, has been widely studied.⁸⁻¹²

Similar to graphite, MoS₂ has layered structure that hexagonal Mo layers are sandwiched in between two hexagonal S layers *via* van der Waals force.^{13, 14} Its layered structure is inherently beneficial for intercalation of lithium ions with high capacity.⁹ But MoS₂ also suffers poor conductivity and structural pulverization as many other anode materials do.^{8, 9, 15} What is worse, Li₂S, one of the lithiation products, can readily react with electrolyte, leading to the capacity fading and inferior rate capability.¹⁶ Three main strategies have been applied to address the challenges: (i) enlarging interlayer distance of MoS₂ (the lattice constant *c*) for easier ions intercalation;¹⁵ (ii) fabricating MoS₂ with various morphology, e.g. nanowires,⁹ nanosheets,^{17, 18} nanoflakes,¹⁹ nanoparticles,²⁰ nanowalls,²¹ nanoplates;²² and (iii) embedding MoS₂ into carbon conductive matrixes for better structural stability and conductivity.^{8, 16, 23, 24} Although the above approaches have been proven more or less effective, there is still plenty of room for further improvement. Another viable solution is to apply porous 3D hierarchical carbon-

based nanocomposites. Consisting of interconnected porous nanoscale building blocks, 3D hierarchical nanostructures not only have advantages of conventional carbon supported nanocomposites where active materials are embedded in dense carbon matrix to obtain enhanced structural stability and electron conductivity, but also possess their own unique properties: the existing pores offer extensive percolation network for increased electrolyte-electrode interface and the space needed for volume expansion, and shorten lithium ion diffusion pathway.^{6, 25} So far, only MoS₂ in dense carbon have been reported. And the synthesis of porous 3D MoS₂ nanocomposites remains a challenge.

Instant gelation, a novel wet chemical method offers the solution. This method takes advantage of the 3D macromolecules in silicate sol which can readily react with selected Mo precursors to form a transparent semisolid “jelly” in few seconds (detailed discussion available in later section). Other small molecules including carbon source and water are trapped inside the cross-linked chains of the jelly. The 3D cross-linked network can be turned into a 3D MoS₂/SiO₂/C dense network in a post annealing step. After the removal of SiO₂, 3D porous MoS₂@C nanocomposites are obtained. The as-prepared composites, having MoS₂ clusters or strips ingrained into carbon matrix as well as massive micro- and mesopores inside, demonstrate excellent electrochemical performance, e.g. stable cyclability, excellent rate performance.

2. Experimental Section

2.1 Preparation of silicate sol: Silicate sol was prepared *via* a modified procedure adapted from literature.²⁶ Briefly, 4.459 mL of TEOS (tetraethyl orthosilicate) and 0.016 mL HCl were added to an ethanol/water mixture (2.16 mL H₂O and 7 mL Ethanol). The molar

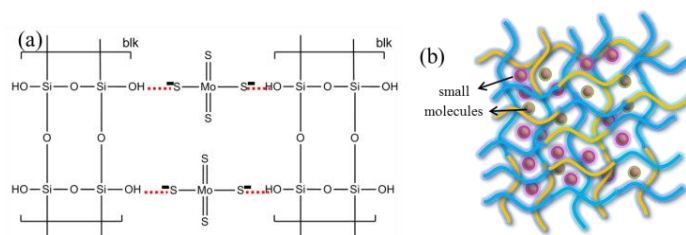
ratio of the four substances is set at: TEOS:H₂O:ethanol:HCl = 1:6:6:0.01. After stirring at 60 °C for 4 h, the silicate sol is immediately used for the instant gelation reaction.

2.2 Preparation of porous 3D MoS₂@C composites: Desirable amount (1.0, 1.5, or 2.0 g) of ammonium tetrathiomolybdate (ATTM) was dissolved in 30 mL of DI water with constant stirring, to which 1.8 g of table sugar was added as carbon source. The mixture was poured into the pre-prepared silicate sol. Within 1 minute, crimson jelly-like semisolids were formed via instant gelation. The samples were dried at room temperature for 5 days to obtain ATTMsilica/sugar composites. The dry samples were then calcined at 800 °C in the forming gas (4 % H₂ in Ar) for 4 h. The reactions that took place during calcination include decomposition of ATTMsilica and carbonization of sugar to produce MoS₂/SiO₂/C dense network. Finally, porous MoS₂@C samples were obtained after removing SiO₂ in 2 M NaOH prepared in DI water/ethanol mixture (1:1 by volume) at 90 °C for 20 h. For convenience, the samples prepared via instant gelation are noted according to the ATTMsilica amount, *i.e.*, 1.0 g as A, 1.5 g as B, and 2.0 g as C. The regular MoS₂ sample (labeled as D) was prepared by direct decomposition of ATTMsilica.

2.3 Characterization: The structure, composition, and morphology of the samples were characterized by X-ray diffraction (XRD, Rigaku Miniflex-II with Cu K α (λ = 1.5406Å) radiation, 30 kV/15 mA current and k β -filter), transmission electron microscopy (TEM; JEOL-2010, 200 kV), and scanning electron microscopy (SEM, S-3400NII) equipped with energy-dispersive X-ray analysis (EDS). Field Emission SEM (FESEM) images were taken by Hitachi S-5200 FEG microscope at 2 kV. The Brunauer-Emmett-Teller (BET) specific surface area of the samples was determined by an ASAP 2020 using the standard N₂ adsorption and desorption isotherm measurements at 77 K. Electrochemical measurements were conducted using CR-2032 coin cells. The working electrode was prepared by casting the slurry (70 wt% of active materials, 20 wt% of carbon black, and 10 wt% of polyvinylidene fluoride binder in N-methyl-2-pyrrolidinone) onto nickel foam, and dried in a vacuum oven at 70 °C for 12 h to remove the solvent. A lithium foil was used as the counter electrode and a mixture of 1 M LiPF₆ in ethylene carbonate (EC)/dimethyl carbonate (DMC) (1:1 by volume) was used as the electrolyte. Cell assembly was carried out in an argon-filled glovebox with oxygen concentration below 1 ppm. The galvanostatic charge/discharge measurements were performed using a Land battery testing system in the voltage window of 0.005-3 V (*vs.* Li⁺/Li). The cyclic voltammetry (CV) and the electrochemical impedance were measured using a Princeton Applied Research Versa STAT4 electrochemical workstation and a CHI-680A (CH Instruments, Inc.) workstation, respectively.

3. Results and discussion

In the instant gelation method, giant silicon-containing macromolecules are formed through the sol-gel process of tetraethyl orthosilicate (TEOS) that undergoes three staged reactions (*e.g.* hydrolysis, condensation, and polymerization) under the presence of water or alcohol. The as-prepared macromolecules contain numerous hydroxyl (-OH) groups which can bind polyatomic anions to form transparent jelly-like semisolids in a short time ranging from a few seconds to 2 or 3 days. Before mixing, the two solutions are freely flowing fluids; but once combined, a jelly-like semisolid is produced due to the formation of a large cross-linked 3D network via numerous hydrogen bonds. A possible microstructure is shown in Scheme 1(a). Small molecules, *e.g.*, water can be readily trapped inside the chains (Scheme 1(b)), similar to the swelling behavior observed in some bulky cross-linked polymers. Finally, the water is evaporated leaving shrunk solids behind.



Scheme 1. (a) Proposed structure of the instant gelation products; (b) Schematic illustration of the products.

The active polyatomic anions in such jelly formation verified so far include MoS₄²⁻, MoO₄²⁻, PO₄³⁻, and MnO₄⁻. All these polyatomic anions have similar structures – a central atom surrounded by S or O atoms. The images of “jelly” formed and the molecular structures of the corresponding polyatomic anions are available in Fig. S1. Nevertheless, other structurally similar anions, like SO₄²⁻, NO₃⁻, can’t form such transparent “jelly”. This could be explained by their higher electronegativity of the central atoms (the electronegativity values for several elements are listed in Table S1). More electronegative S and N, as compared with P, Mn and Mo, decrease the ionic character of the bond in SO₄²⁻ and NO₃⁻, thus diminish the strength of their hydrogen bonding with the macromolecules. The strength of hydrogen bond also correlates with the gelation time. For example, the gelation takes no more than 30 s for MoS₄²⁻ but almost 2 days with PO₄³⁻.

When subjected to post calcination or annealing process in different atmosphere, such jelly-like semisolids can be used to prepare a variety of products including metal oxides, metal sulfides, and metal nitrides. Moreover, the method can be extended to the preparation of nanocomposites with integrated properties by simply adding other desired components. After calcination, the silicate network turns into SiO₂, which can be removed by NaOH or HF, thus resulting in a final product with high surface area because of the micro-, and mesopores inside. Porous compounds with high surface area are very promising materials for applications as catalysts and electrode materials. In this paper, this method is applied for the preparation of MoS₂ with properties suitable for the application as anode material in lithium ion batteries. In detail, four samples are analyzed, and their information is available in experimental section.

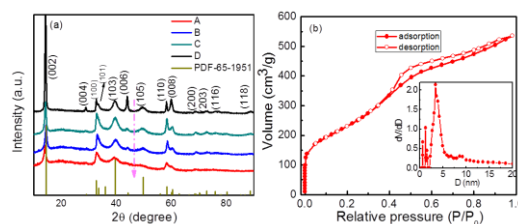


Figure 1. (a) XRD patterns of the samples A, B, C, and D; (b) N₂ adsorption/desorption isotherm of sample A at 77 K.

Table 1. Properties of the four samples

samples	C (wt %)	BET surface area (m ² g ⁻¹)
A: MoS ₂ @C	72.6	853.2
B: MoS ₂ @C	60.0	419.0
C: MoS ₂ @C	44.8	228.5
D: MoS ₂	0	6.5

The XRD patterns of the four samples are shown in Fig. 1(a). All diffraction peaks of the four samples can be assigned to hexagonal MoS₂ (JCPDS 65-1951). No other phases can be detected. Pure MoS₂ (sample D) has all the peaks identifiable with high intensities. However, the MoS₂@C samples have their peaks broadened to the extent that some are totally disappeared, e.g., (004); while others have their intensity counter correlated with the carbon content: the more carbon amount, the less the peak intensity (see the trend demonstrated by the pink dashed line). The specific surface area were measured from the N₂ adsorption/desorption isotherms at 77 K and one of them (sample A) is given in Fig.1(b), while others in Fig.S2. The Brunauer-Emmett-Teller (BET) surface area are listed in Table 1. Note that the value for sample A MoS₂@C is 853.2 m² g⁻¹, which appears the highest value so far for MoS₂ based materials, much higher than those reported in literature: 138 m² g⁻¹ of the hierarchical hollow nanoparticles,²⁰ 81 m² g⁻¹ of 1D MoS₂-C nanotubes and 14 m² g⁻¹ of the MoS₂-C nanowires,⁹ 38 m² g⁻¹ of MoS₂@CMK-3 nanocomposite,⁸ 4.89 m² g⁻¹ of raw MoS₂ and 9.83 m² g⁻¹ of restacked MoS₂.¹⁵ From the pore distribution curve (the inset of Fig.1(b)), both micro-, and mesopores co-exist in the sample, and majority of them have a pore size around 4 nm. The tendency that the BET surface areas of MoS₂@C samples increases with the carbon amount (see Table 1) suggests the pores are mainly existed in the carbon matrix.

SEM images in Fig. 2 show the morphology of as-prepared products over a large area. The bare MoS₂ mainly consists of large lumps (Fig. 2(a)). Once table sugar is introduced to the solution containing polyatomic anions, the final products have MoS₂ clusters embedded into the carbon matrix. In sample A, the MoS₂ clusters are not stacked with each other (see Fig. 2(b)) because of the low MoS₂ content. Increasing the amount of MoS₂ in sample B leads to more pronounced clusters (Fig. 2(c)), which are nearly touching each other. The ratio of MoS₂ and carbon appears close to optimal in sample B. Because further increasing of MoS₂ (sample C) leaves some MoS₂ lumps on the surface of the composite architecture (see Fig. 2(d)). FESEM images of sample B in Fig. 2(e, f) reveal that there are also smaller clusters (besides those separated large ones) continuously distributed in carbon, leading to the fluffy surface of carbon. The carbon content of the samples were determined by EDS and summarized in Table 1, with the weight percentage of 72.6, 60.0, and 44.8 in samples A, B, and C, respectively.

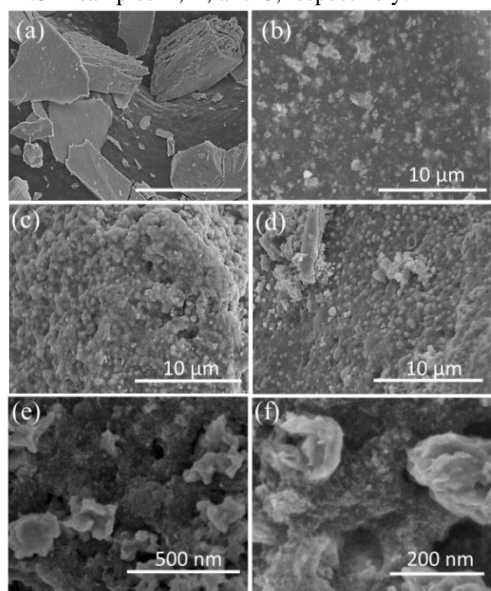


Figure 2. SEM images of (a) MoS₂, sample D; and MoS₂@C (b) A; (c) B; (d) C; (e) and (f) FESEM images of sample B.

TEM images of bare MoS₂ and MoS₂@C composites are presented in Fig. 3. As can be seen in Fig. 3a, the bare MoS₂ mainly contains irregular flakes or spheres. The MoS₂@C samples have MoS₂ clusters or strips well embedded in carbon (Fig. 3(b-d)). When the fraction of MoS₂ is small, only separated clusters with diameters over 80 nm are presented (sample A in Fig. 3(b)). In samples B and C, where MoS₂ content is higher, both the clusters and the leaf-like MoS₂ strips are observed in the carbon matrix (Fig. 3(c, d)). Unlike the distinguishable clusters in sample A, the strips and clusters in B and C tend to densely pack together without clear boundaries. The HRTEM images in Fig. 3(e, f) display both, clusters and strips, have the typical MoS₂ layered structure ingrained into carbon. The interlayer of the clusters and strips have the spacing of ca. 0.63 and 0.62 nm, respectively, corresponding to the interplanar distance for (002) plane of hexagonal MoS₂.

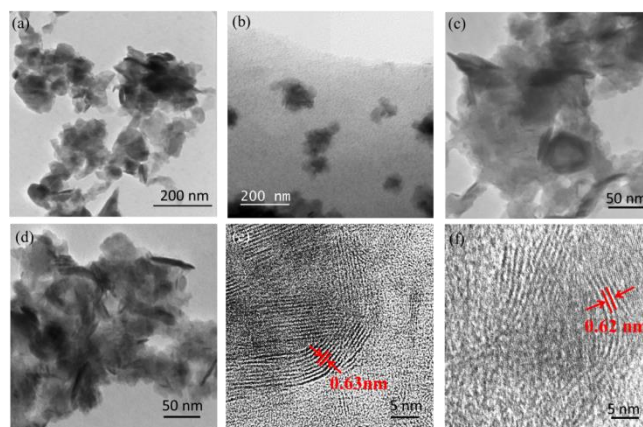


Figure 3. TEM images of (a) bare MoS₂, sample D; and MoS₂@C nanocomposites (b) A; (c) B; (d) C; HRTEM of MoS₂ clusters (e) and strips (f) from sample B.

Thus prepared materials were assembled into half-cells and evaluated by galvanic charging/discharging in the voltage range of 0.005-3 V (vs. Li⁺/Li) at a current density of 100 mA g⁻¹. The first three charge and discharge voltage profiles of all samples are shown in Fig. 4. As can be seen, two distinguishable plateaus at ~1.1 V and ~0.6 V were observed in the initial discharge cycles, which correspond to the insertion of Li ions into the S slab to form Li-S bonds and the reduction of Mo⁴⁺ into Mo metal particles, respectively.^{9, 15, 24, 27} In the subsequent discharge processes, two plateaus around 2.0 V and 1.1 V arise but the plateau at 0.6 V from the first discharging cycle disappears. The plateau at ~2.0 V corresponds to the formation of gel-like polymeric layers.^{15, 16, 23} The charging (delithiation) process displays a plateau around 2.2 V, corresponding to the possible reactions of Mo and Li₂S to form S or MoS₂.^{16, 20} The charge and discharge profiles agree well with the previous reports.^{8, 16, 20, 24, 27} Noticeably, the carbon content has a great influence on the plateaus: the more MoS₂ in the electrode materials (from sample A to D), the broader are the plateaus. Cyclic voltammetry, as a widely accepted method for investigation of redox couples, is also applied to study the redox reactions in the electrodes. As demonstrated in Fig. 4(e) and Fig. S3, two large reduction peaks at 0.9 V and 0.25 V in the initial cycle were observed for all samples. The peak at 0.9 V is attributed to the structure transformation of MoS₂ from the 2H (trigonal prismatic coordination) to the 1T (octahedral coordination) upon Li intercalation into the S slabs.^{8, 15, 16, 24} The 0.25 V peak indicates the reduction of Mo⁴⁺ to Mo nanoparticles and formation of the solid electrolyte interphase (SEI) layer from electrochemically driven

electrolyte degradation.¹⁷ In the subsequent discharge cycles, a new reduction peak around 1.85 V emerges corresponding to formation of the sulfur-related materials.^{8, 23} In the anodic sweeps, a pair of peaks (the inconspicuous one at 1.6 V, and the distinct one at 2.4 V) is related to the conversion of Mo and Li_2S to S or MoS_2 .^{8, 16, 20, 22} The CV results show a good consistency with the charge-discharge plateaus described above except for small variation between the positions of CV peaks and the plateaus, likely due to a high scan rate used in CV. Similar variation has been observed before.²⁴ Notably, opposite to the CV curves of bare MoS_2 (sample D) in Fig. S3(c), carbon-containing samples perfectly reproduce after the initial cycle (see Fig. 4(e), S3(a) and S3(b)), indicating that carbon matrix improves structural stability of the materials and cyclability of the electrodes.

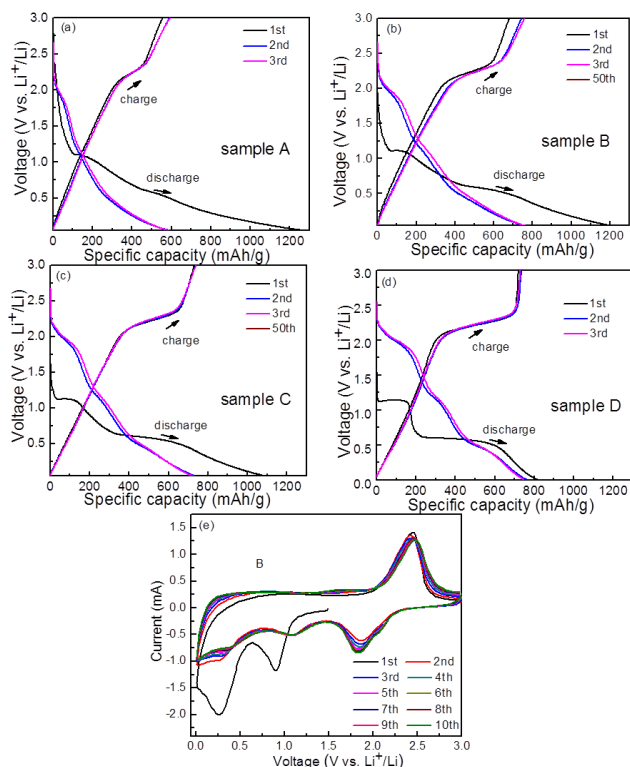


Figure 4. Voltage profiles of samples: (a) A, (b) B, (c) C, and (d) D at a current density of 100 mA g^{-1} ; (e) cyclic voltammetry profiles of sample B.

The cyclic performance of the four samples at a current density of 100 mA g^{-1} in the voltage window of 0.005-3 V vs Li^+/Li is displayed in Fig. 5(a). The initial lithiation (discharge) capacity for A, B, C, and D samples are 1405.7, 1281.6, 1155.3, and 814.4 mAh g^{-1} , respectively, with the corresponding charge capacities 555.7, 679.6, 731.3, and 719.8 mAh g^{-1} , giving the initial Coulombic efficiency of 39.5 % for A, 53 % for B, 63.3 % for C, and 88.4 % for D. The low initial Coulombic efficiency is caused by the irreversible consumption of lithium ions due to the formation of SEI layers. From the cyclic performance curve, the three $\text{MoS}_2@C$ nanocomposites have more stable cyclic capacity than that of bare MoS_2 . After 50 cycles, samples A, B, and C still have discharge capacities remained at 491.4, 657.1, 608.8 mAh g^{-1} , higher than that of bare MoS_2 (394.5 mAh g^{-1}). Because of its optimal MoS_2 to carbon ratio, sample B exhibits the best cyclic performance among the composites. Part of the cyclic performance information of the four samples is summarized Table S2 for comparison. Fig. 5(b) shows the Coulombic efficiency for the first 20 cycles of the four

samples. Notice that there is a clear tendency in the first 10 cycles that the higher the carbon amount, the lower the Coulombic efficiency is. The difference may be due to the larger surface area in the high carbon-containing samples exposed to electrolyte for the formation of larger SEI layers. After the initial 10 cycles, the Coulombic efficiency of the four samples is fairly close to each other, remaining above 97 %. Fig. 5(c) displays the rate performance of the $\text{MoS}_2@C$ composites at different current densities. Again, sample B demonstrates a better rate performance. As expected, its specific capacity decreases with increasing the current density: the electrode delivered a capacity of $\sim 650 \text{ mAh g}^{-1}$ at 200 mA g^{-1} , $\sim 580 \text{ mAh g}^{-1}$ at 300 mA g^{-1} , $\sim 510 \text{ mAh g}^{-1}$ at 500 mA g^{-1} , $\sim 440 \text{ mAh g}^{-1}$ at 800 mA g^{-1} , and $\sim 410 \text{ mAh g}^{-1}$ at 1000 mA g^{-1} , respectively. When the current density was changed to 100 mA g^{-1} , the specific capacity rebounded to $\sim 700 \text{ mAh g}^{-1}$, showing negligible capacity loss. Electrochemical impedance helps in understanding the effect of $\text{MoS}_2@C$ nanocomposites structure on the kinetics of the electrochemical reaction. As seen in Fig. 5(d), the Nyquist plots for both B and D electrodes consist of semicircles with the charge-transfer resistance from the electrode interface and the passivating SEI layer, while the straight line (Warburg line) in the low frequency region is attributed to lithium ion diffusion. The smaller semicircle for $\text{MoS}_2@C$ suggests a lower electrochemical reaction resistance. This fact indicates that the interconnected porous carbon scaffold can increase the conductivity and ensure fast overall charger-transfer kinetics of the electrodes.

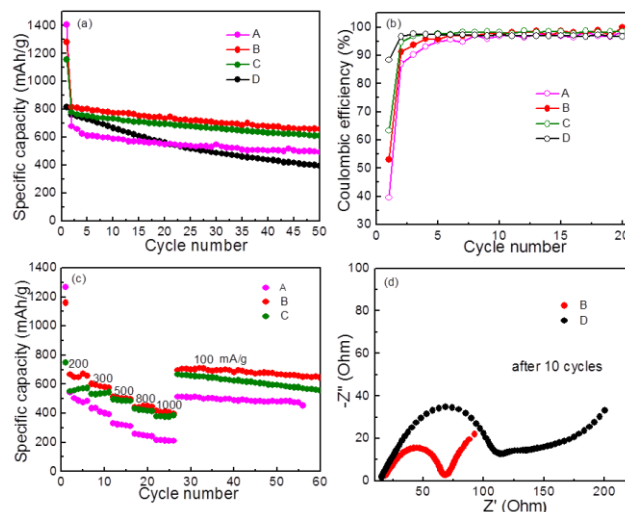
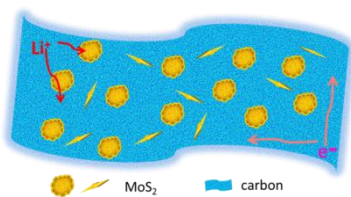


Figure 5. (a) Cycle performance of the four samples at a current density of 100 mA g^{-1} ; (b) Coulombic efficiency of the first twenty cycles of the four samples; (c) rate performance of A, B, C; (d) Nyquist plots of B and D at zero bias obtained after 10 charge and discharge cycles.

The improved electrochemical performance of $\text{MoS}_2@C$ can be attributed to the unique nanocomposites architecture of MoS_2 clusters or strips embedded in the carbon (Scheme 2). The carbon scaffold not only acts as a conductive matrix which promotes fast electron transports, but also maintains structural integrity of the electrode materials, despite large volume changes during the charging and discharging cycles, as well as, hinders aggregation of MoS_2 clusters or strips.²⁸ The high surface area provides large effective area for a better contact between the electrode materials and electrolyte. Additionally, the large amount of pre-existing micropores and mesopores inside the materials not only facilitates the rate-limited ion diffusion to active sites with less resistance, but also provides the space needed for MoS_2 volume expansion.²⁹

Therefore, the rationally designed porous 3D nanocomposites are very promising as electrode materials.



Scheme 2. Schematic illustration of the micro-, and mesoporous nanostructure, that beneficially contributes to fast ion diffusion and electron transport kinetics.

4. Conclusion

In summary, a novel synthetic route – instant gelation, was developed for the first time to synthesize 3D MoS₂@C nanocomposites. The as-prepared nanocomposites have layered MoS₂ clusters or strips integrated into conductive carbon matrix. The interconnected carbon matrix not only acts as a highway for the electron transport, but also ensures the structural stability of the materials during charging and discharging. Large amount of micro- and mesopores inside the materials also effectively shorten the rate-limited ion diffusion path. Owing to the excellent stability and fast electron and ion transport kinetics, the MoS₂@C nanocomposites demonstrate excellent electrochemical properties with high specific capacities and stable charge/discharge performance. Moreover, the composites prepared by instant gelation have high specific surface area, which make it also very promising for other applications, such as catalysts.

Acknowledgements

We acknowledge the funding support from NSF/CMMI NanoManufacturing Program under Grant No. 1131290 and the office of Vice President for Research at NMSU. L.F. acknowledges the Preparing Future Faculty Graduate Assistantship Award. This work is partially supported by the U.S. Department of Energy, Office of Basic Energy Sciences, Division of Materials Sciences and Engineering. Sandia is a multiprogram laboratory operated by Sandia Corporation, a wholly owned subsidiary of Lockheed Martin Corporation, for the U.S. Department of Energy's National Nuclear Security Administration under Contract DE-AC04-94AL85000.

Notes and references

^aDepartment of Chemical Engineering, New Mexico State University, Las Cruces, New Mexico 88003, United States.

^bAdvanced Materials Laboratory, Sandia National Laboratories, Albuquerque, New Mexico 87106, United States.

^cDepartment of Chemistry and Biochemistry, New Mexico State University, Las Cruces, New Mexico 88003, United States.

Corresponding Author: *Tel: 575-646-4204, Fax: 575-646-7706. E-mail: hluo@nmsu.edu (H. Luo)

Electronic Supplementary Information (ESI) available: [pictures of the “jelly” formed from different polyatomic anions, table of electronegativity values of a few elements, N₂ adsorption/desorption isotherm of samples B, C, D at 77 K, cyclic voltammetry profiles of A, C, D, table of selected cyclic performance information of the four samples]. See DOI: 10.1039/b000000x/

1. C. He, S. Wu, N. Zhao, C. Shi, E. Liu and J. Li, *ACS Nano*, 2013, **7**, 4459.
2. B. Dunn, H. Kamath and J.-M. Tarascon, *Science*, 2011, **334**, 928.
3. Y. Xu, R. Yi, B. Yuan, X. Wu, M. Dunwell, Q. Lin, L. Fei, S. Deng, P. Andersen, D. Wang and H. Luo, *J Phys. Chem.Lett.*, 2012, **3**, 309.
4. H. B. Wu, J. S. Chen, H. H. Hng and X. Wen Lou, *Nanoscale*, 2012, **4**, 2526.
5. L. Fei, Q. Lin, B. Yuan, G. Chen, P. Xie, Y. Li, Y. Xu, S. Deng, S. Smirnov and H. Luo, *ACS Appl. Mater. Interfaces* 2013, **5**, 5330.
6. D. D. Vaughn, 2nd, O. D. Hentz, S. Chen, D. Wang and R. E. Schaak, *Chem. Commun.*, 2012, **48**, 5608.
7. X. Zhou, Y.-X. Yin, L. J. Wan and Y. G. Guo, *J. Mater. Chem. A*, 2012, **22**, 17456.
8. X. Zhou, L. J. Wan and Y. G. Guo, *Nanoscale*, 2012, **4**, 5868.
9. C. Zhang, Z. Wang, Z. Guo and X. W. Lou, *ACS Appl.Mater. Interfaces*, 2012, **4**, 3765.
10. Y. Li, H. Wang, L. Xie, Y. Liang, G. Hong and H. Dai, *J Am Chem Soc*, 2011, **133**, 7296.
11. X. Zong, H. Yan, G. Wu, G. Ma, F. Wen, L. Wang and C. Li, *J Am Chem Soc*, 2008, **130**, 7176.
12. R. Rosentsveig, A. Margolin, A. Gorodnev, R. Popovitz-Biro, Y. Feldman, L. Rapoport, Y. Novema, G. Naveh and R. Tenne, *J. Mater. Chem. A*, 2009, **19**, 4368.
13. Z. Wang, T. Chen, W. Chen, K. Chang, L. Ma, G. Huang, D. Chen and J. Y. Lee, *J. Mater. Chem. A*, 2013, **1**, 2202.
14. C. Zhang, H. B. Wu, Z. Guo and X. W. Lou, *Electrochem. Commun*, 2012, **20**, 7.
15. G. Du, Z. Guo, S. Wang, R. Zeng, Z. Chen and H. Liu, *Chem.Commun.*, 2010, **46**, 1106.
16. X. Zhou, L. J. Wan and Y. G. Guo, *Chem. Commun.*, 2013, **49**, 1838.
17. S. Ding, D. Zhang, J. S. Chen and X. W. Lou, *Nanoscale*, 2012, **4**, 95.
18. S. Ding, J. S. Chen and X. W. Lou, *Chem.-Eur. J.*, 2011, **17**, 13142.
19. C. Feng, J. Ma, H. Li, R. Zeng, Z. Guo and H. Liu, *Mater. Res. Bull.*, 2009, **44**, 1811.
20. M. Wang, G. Li, H. Xu, Y. Qian and J. Yang, *ACS Appl. Mater. Interfaces*, 2013, **5**, 1003.
21. U. K. Sen and S. Mitra, *ACS Appl. Mater. Interfaces*, 2013, **5**, 1240.
22. H. Hwang, H. Kim and J. Cho, *Nano. Lett.*, 2011, **11**, 4826.
23. Q. Wang and J. Li, *J. Phys. Chem.C*, 2007, **111**, 1675.
24. K. Chang and W. Chen, *ACS Nano*, 2011, **5**, 4720.
25. A. Magasinski, P. Dixon, B. Hertzberg, A. Kvit, J. Ayala and G. Yushin, *Nature Mater.*, 2010, **9**, 353.
26. Q. Hu, J. Pang, N. Jiang, J. E. Hampsey and Y. Lu, *Microporous Mesoporous Mater.*, 2005, **81**, 149.
27. J. Xiao, D. Choi, L. Cosimbescu, P. Koech, J. Liu and J. P. Lemmon, *Chem. Mater.*, 2010, **22**, 4522.
28. S. Xin, Y. G. Guo and L. J. Wan, *Acc. Chem. Res.*, 2012, **45**, 1759.
29. L. Shen, E. Uchaker, C. Yuan, P. Nie, M. Zhang, X. Zhang and G. Cao, *ACS Appl. Mater. Interfaces*, 2012, **4**, 2985.

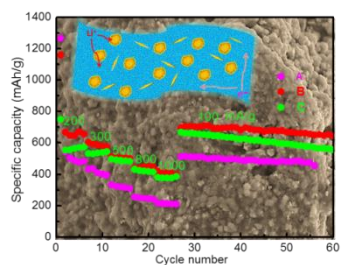


Table of content: Instant gelation prepared porous MoS₂@C nanocomposites show excellent electrochemical properties due to their excellent stability and fast electron and ion transport kinetics.